Pharm Res (2015) 32:1288–1303
DOI 10.1007/s11095-014-1533-x

RESEARCH PAPER

Intestinal Uptake and Transport of Vitamin B_{12}-loaded Soy Protein Nanoparticles

Jing Zhang • Catherine J. Field • Donna Vine • Lingyun Chen

Received: 22 July 2014 / Accepted: 25 September 2014 / Published online: 16 October 2014

ABSTRACT

Background Intestinal absorption of vitamin B_{12} (VB_{12}) is a major challenge in combating pernicious anemia due to intrinsic factor (IF) deficiency.

Purpose The aim of this study was to explore the feasibility of using soy protein isolates (SPI) nanoparticles to improve the intestinal transport and absorption of VB_{12}.

Methods Three different sized VB_{12}-loaded SPI nanoparticles were produced by modulating preparation conditions using a cold-gelation method. The intestinal uptake and transport mechanisms of SPI nanoparticles for VB_{12} delivery were investigated and related to particle size.

Results SPI nanoparticles were not cytotoxic to Caco-2 cells and were effectively internalized into the cytoplasm *via* multiple endocytosis pathways including clathrin- and/or caveolae-mediated endocytosis and macropinocytosis routes. VB_{12} transport across the Caco-2 cell monolayers was increased to 2–3 times after nanoencapsulation, which was dependent on particle size, in the increasing order of 30 > 100 > 180 nm. Using inhibitor block method, the transport of 30 and 100 nm SPI nanoparticles appeared to be clathrin-mediated transcytosis and macropinocytosis routes. The intestinal transport of VB_{12}, assessed using rodent jejunum in Ussing chambers, was improved up to 4-fold after being encapsulated into 30 nm SPI nanoparticles.

Conclusions The findings suggest that SPI nanoparticles could be a promising carrier to facilitate the oral delivery of VB_{12}.

KEY WORDS Caco-2 cells · intestinal transport · particle size · soy protein nanoparticles · vitamin B_{12}

ABBREVIATIONS

COL	Colchicine
COUM-6	Coumarin 6
CPZ	Chlorpromazine hydrochloride
CyD	Cytochalasin D
DAPI	4′, 6-Diamidino-2-phenylindole
DLS	Dynamic light scattering
DMEM	Dulbecco's modified eagle medium
DMSO	Dimethyl sulfoxide
FBS	Fetal bovine serum
FI	Fluorescence intensity
FLI	Flilipin III
HBSS	Hank's balanced salt solution buffer
HEPES	4-(2-Hydroxyethyl)-1-piperazineethanesulfonic acid
IF	Intrinsic factor
LC	Loading capacity
LE	Loading efficiency
PBS	Phosphate buffered saline
PLGA	Poly(lactic-co-glycolic) acid
PMS	Phenazine methosulfate
SPI	Soy protein isolates
TEER	Transepithelial electrical resistance
VB_{12}	Vitamin B_{12}
VD_3	Vitamin D_3
WGA	Wheat germ agglutinin
XTT	2,3-bis-(2-methoxy-4-nitro-5-sulphenyl)-(2H)-tetrazolium-5-carboxanilide

J. Zhang • C. J. Field • D. Vine • L. Chen (✉)
Department of Agricultural, Food and Nutritional Science, University of Alberta, Edmonton, Alberta T6G 2P5, Canada
e-mail: lingyun.chen@ualberta.ca

INTRODUCTION

Nutraceuticals are frequently supplemented in functional foods in order to achieve enhanced health benefits. However, the bioavailability and efficacy of many nutraceutical compounds are limited due to the chemical formulation and poor transport across the intestinal mucosa. Vitamin B_{12} (VB_{12}) is a water-soluble nutraceutical; however, its absorption is a complex and multistep process. Firstly, dietary VB_{12}, which is usually bound to proteins in food, is released in the stomach

under the effects of gastric acid and pepsin. The free VB_{12} then binds to haptocorrin (HC), which is a carrier produced by salivary glands and parietal cells in the stomach. [1] When the VB_{12}-HC complex reaches the duodenum, HC is degraded by pancreatic protease, the liberated VB_{12} then binds to intrinsic factor (IF) produced by parietal cells. [2] In the distal ileum, after being recognized by specialized receptors on mucosal cells, IF-VB_{12} complex enters the blood and is directed to portal circulation. In a healthy adult, about 50% of dietary VB_{12} is absorbed in the intestine. [3] However, this rate of absorption can be significantly reduced by alterations in gastric acidity, intrinsic factor (IF) production and damage in the terminal ileum where IF-VB_{12} complex is absorbed. [1] Novel methods of oral delivery that do not rely on the complex intraluminal and epithelial processes for transport are needed to combat the growing portion of the population that has marginal VB_{12} status [1, 4].

Nanoparticles have the potential to adhere to the intestinal mucus layer by non-specific interactions and to pass through this barrier to interact with the intestinal epithelium. [5, 6] Nanoparticle formulations have been shown to promote the translocation of nutraceuticals across the intestinal epithelium *via* paracellular and transcellular routes. [7] There have been substantial advances achieved in nanoparticle engineering to enhance the oral bioavailability of hydrophobic compounds such as β-carotene and vitamin D by increasing their solubility and stability in GI tract; however, few studies have been done to promote the absorption of hydrophilic nutraceuticals such as VB_{12} using nanoparticles as carriers [8].

Soy protein isolates (SPI) are one of the promising candidates for preparing nanoparticles delivery systems due to their biodegradable, biocompatible, high-nutritive and excellent gelation properties. [9] SPI nanoparticles have been prepared using the desolvation method to encapsulate curcumin and vitamin D_3 (VD_3). [10–12] However, the utilization of organic reagents such as ethanol, glutaraldehyde, dimethyl sulfoxide, and N-(3-dimethylaminopropyl)-N-ethylcarbodiimide in preparation of SPI nanoparticles has limited their application in food products. We have developed a novel cold-gelation method that does not require the use of organic solvents to prepare SPI nanoparticles and these particles demonstrate uniform size distribution, ability to adjust size and good stability. [13] The molecular interaction between soy protein and VB_{12} has been investigated. [14] These findings suggested that soy protein had the ability to bind VB_{12} into a three-dimensional protein network mainly *via* hydrophobic interactions [14] and soy protein may be a potential carrier for VB_{12} to improve its bioavailability. The aim of this study was to explore the feasibility of using SPI nanoparticles to improve the intestinal transport and absorption of VB_{12}.

As particle size is an important parameter determining nanoparticle efficacy,[15] three different sized VB_{12}-loaded SPI nanoparticles were prepared according to our previous work [13] and the impact of particle sizes on the cellular uptake and transport properties were investigated. Caco-2 cell monolayers were used as an *in vitro* model to mimic the small intestinal epithelium. The particle size with optimized VB_{12} transport efficiency was used in an *ex vivo* intestinal Ussing model to determine intestinal transport. The intestinal uptake and transport mechanisms were identified and related to particle size.

MATERIALS AND METHODS

Materials

SPI (PRO-FAM® 646) was kindly provided by Archer Daniels Midland Company (ADM, Decatur, IL, USA). It contained 94.4% protein on a dry basis. Dimethyl sulfoxide (DMSO), 2,3-bis-(2-methoxy-4-nitro-5-sulphenyl)-(2H)-tetrazolium-5-carboxanilide (XTT) assay kit with 1% phenazine methosulfate (PMS), Coumarin 6 (COUM-6), Corning® Costar® cell culture plates, 4′, 6-diamidino-2-phenylindole (DAPI), flilipin III (FLI), colchicine (COL), chlorpromazine hydrochloride (CPZ) and cytochalasin D (CyD) were purchased from Sigma-Aldrich (Oakville, ON, Canada). Wheat germ agglutinin (WGA)-Alexa Fluor® 555 conjugate, Dulbecco's modified eagle medium (DMEM), fetal bovine serum (FBS), trypsin-EDTA, 4-(2-hydroxyethyl)-1-piperazineethanesulfonic acid (HEPES) and 1% antibiotic-antimycotic were purchased from Invitrogen (Burlington, ON, Canada). Cobalt reference standard solution was purchased from Fisher Scientific (Toronto, ON, Canada). Caco-2 cells (HTB®-37™) were purchased from the American Type Culture Collection (ATCC, Manassas, VA, USA). All other chemicals were of reagent grade.

SPI Treatment and Labeling

Pretreated SPI solution was prepared according to our previous procedure. [13] For a better observation, a portion of pre-treated SPI was labeled with COUM-6. Briefly, 1 μg/ml COUM-6 in DMSO was added in pre-treated SPI solution at pH 9, where the dye is chemically stable. After stirring overnight in a dark environment at 4°C, the solution was dialyzed against 5 L of phosphate buffered saline (PBS) (0.01 M, pH7.4), the PBS being replaced every 6 h for 6 days until no COUM-6 was detected in solution by a Fluorescence spectrophotometer (SpectraMax M_3, Sunnyvale, CA) at λ_{ex}= 458 and λ_{em}=505 nm. The amount of COUM-6 was calculated based on a standard calibration curve constructed by measuring the fluorescence emission intensity of the COUM-6 at different concentrations (0.1–1.5 μg/ml) using pre-treated SPI as a reaction medium.

Preparation of VB_{12}-loaded Nanoparticles

VB_{12} (10 μg/ml) was introduced into pre-treated SPI solutions at pH 8 and pH 9 and left to react at room temperature overnight, followed by the addition of $CaCl_2$ dropwise to induce nanoparticle formation. [13] The unbound VB_{12} was removed after dialysis at 4°C against 5 L of PBS, which was replaced every 6 h for 4 days until no free VB_{12} was detected in the outer solution Atomic absorption spectra (Varian Australia Pty Ltd, Mulgrave Victoria, Australia). VB_{12}-loaded SPI nanoparticles were collected after dialysis. The amount of loaded VB_{12} was measured by Atomic absorbance spectra using cobalt reference standard solution (Fisher Scientific, Toronto, ON, Canada) to make a standard curve of [Co] *vs.* Absorbance. The loading capacity (LC, %) and efficiency (LE, %) were calculated *via* Eqs. (1) and (2) respectively:[16]

$$\mathrm{LC}\ (\%) = \frac{\mathrm{VB_{12}(\mu g)in\ nanoparticles}}{\mathrm{nanoparticles(\mu g)}} \times 100\% \quad (1)$$

$$\mathrm{LE}(\%) = \frac{\mathrm{VB_{12}(\mu g)\ in\ nanoparticles}}{\mathrm{VB_{12}(\mu g)added}} \times 100\% \quad (2)$$

Characterization of Nanoparticles

The size and zeta-potential of nanoparticles were determined using dynamic light scattering (DLS) and laser Doppler velocimetry using Zetasizer Nano ZS (Malvern Instruments Ltd., UK) at 20°C. The surface morphology of nanoparticles was observed by transmission electron microscopy (TEM, Hitachi H-7000, Japan) [13].

Cell Culture

Caco-2 cells (HTB®-37™, ATCC, Manassas, VA, USA) of passages between 20 and 40 were used. The cells were cultured in DMEM-20, supplemented with 20% FBS, 1% non-essential amino acids, 1% antibiotic-antimycotic and 25 mM HEPES (Invitrogen, Burlington, ON, Canada). Cells were cultured in a humidified atmosphere containing 5% CO_2 at 37°C and the medium was renewed every other day.

XTT Colorimetric Assay

Caco-2 cells were seeded at 5×10^4 cells/well into a 96-well plate in the EMEM-20. The cells were allowed to recover for 24 h at 37°C. The medium in each well (200 μl/well) was then replaced with SPI nanoparticle suspension, diluted with Hank's balanced salt solution buffer (HBSS, pH 7.2) to obtain SPI concentrations of 0.625, 1.25, and 2.25 mg/ml. HBSS treatment without nanoparticles was used as a negative control. After 6 h incubation, cells were washed twice with 200 μl of HBSS after the removal of nanoparticles. Then, 50 μl of 1 mg/ml XTT with 1% PMS mixture (Sigma-Aldrich, Oakville, ON, Canada) was added to each well. The microplates were incubated at 37°C for 2 h in the dark to develop formazan product and read at 450 nm using a Fluorescence spectrophotometer. The absorbance at 690 nm was read as a background. Cell viability (%) was calculated according to Eq. (3):

$$\text{Cell viability}(\%) = \frac{A_{450nm\ 1} - A_{690nm\ 1}}{A_{450nm} - A_{690nm}} * 100\% \quad (3)$$

where $A_{450nm\ 1}$ and A_{450nm} refer to the absorbance value at 450 nm with the treatment of nanoparticles and HBSS buffer respectively. $A_{690nm\ 1}$ and A_{690nm} represent the absorbance value at 690 nm with the treatment of nanoparticles and HBSS respectively.

Cell Counting

The cells were cultured in a T-25 flask, until they came to 80% confluence. The same samples and treatments as indicated in XTT assay were then applied to Caco-2 cells. After 6 h, cells were trypsinized after the removal of nanoparticles, harvested and suspended in 5 ml of DMEM-10. The number of living cells after each treatment was counted by a TC 10^{TM} Automated Cell Counter (Bio-Rad, Singapore) and the data were expressed as number of living cells per ml.

Confocal Laser Scanning Microscopy (CLSM) Study

Caco-2 cells (5×10^5 cells/well) were seeded onto the coverslip in 6-well plates and incubated until 100% confluence was reached. The cells were equilibrated with HBSS at 37°C for 30 min; the buffer was then replaced with 1.5 ml COUM-6 labeled particle suspensions (containing 1.25 mg/ml SPI nanoparticles (w/v)) and further incubated for 6 h. At the end of experiments, the monolayers were washed 3 times with PBS. Cell membranes were stained with 5 μg/ml (w/v) WGA-Alexa Fluor® 594 conjugate in PBS for 10 min at 37°C. After washing three times, Caco-2 cells were then fixed with an ice-cold solution of 3.7% formaldehyde for 30 min at 4°C. Nuclei were stained by 1 μg/ml DAPI. The slides with seeded cells were covered with glycerol (10% in PBS) and closed with cover glasses. Cells were then observed with a CLSM 510 Meta (Carl Zeiss, Jena, Germany) equipped with a diode at 405 nm of excitation, an Argon laser (providing the exCitation at 488 nm) and a helium/neon laser (providing the excitation at 543 nm). An oil immersion objective (40 ×) was used to

visualize samples. Images were processed with ZEN 2009 LE software (Carl Zeiss MicroImaging GmbH, Germany).

Flow Cytometry

Caco-2 cells (5×10^5 cells/well) were seeded in 6-well plates. Upon reaching confluence, the culture medium was replaced by HBSS and pre-incubated at 37°C for 30 min. After equilibration, COUM-6 labeled nanoparticle suspensions (1.5 ml, containing 1.25 mg/ml SPI nanoparticles in HBSS) were added and incubated for 4 h. After removal of nanoparticles, cells were trypsinized, harvested and suspended in FCS washing buffer. Thereafter, the cells were analyzed by a Flow cytometry using FACSCalibur (Becton Dickinson, San Jose, CA, USA). [17] The fluorescence intensity was analyzed by FCS Express 4 Flow Cytometry (De Novo Software, Los Angeles, CA, USA).

Spectrofluorimetry Study

Caco-2 cells (1×10^5 cells/well) were seeded in 48-well plates. Upon reaching confluence, Caco-2 cells were incubated in HBSS at 37°C for 30 min. After equilibration, cellular uptake of nanoparticles was started by exchanging HBSS with 0.4 ml of COUM-6 labeled nanoparticle suspensions (0.625–2.25 mg/ml in HBSS). The incubation of nanoparticles with cells at 37°C lasted for 0.5–4 h. The experiment was terminated by gently washing cell monolayers 3 times with HBSS, 0.4 ml HBSS was then added to each well. Cells were lysed with 0.4 ml Triton X-100 (1% in 0.4 M NaOH). The lysis was analyzed using a microplate reader at λ_{ex}=458 and λ_{em}= 505 nm. The same treatment was applied to the cells without the removal of the nanoparticles, which were used as the corresponding overall. The cells incubated with HBSS were used as a control. Results of cellular uptake efficiency were expressed *via* Eq. 4: [18]

$$\text{Uptake efficiency } (\%) = 100\% \times \frac{FI_1 - FI_2}{FI_3 - FI_4} \tag{4}$$

where FI_1 and FI_2 represent the fluorescence intensity (FI) of the lysed cell solution after removing nanoparticles and HBSS respectively; FI_3 and FI_4 represent the FI of lysed cell solution without removing nanoparticles and HBSS respectively.

Metabolic and Endocytosis Inhibition

To study the potential uptake pathways of nanoparticle, cells were pre-treated with inhibitors including 100 mM NaN_3, 5 μg/ml Colchicine (COL), 10 μg/ml Cytochalasin D (CyD) (Sigma-Aldrich, Oakville, ON, Canada) for 30 min, followed by the incubation with nanosuspension for 4 h. COL and CyD applied were to inhibit the clathrin- and/or caveolae-mediated endocytosis pathways [19]. The cells were washed three times with HBSS after the removal of nanoparticles. Subsequently, HBSS (0.4 ml) and 1% Triton X-100 in 0.4 M NaOH (0.4 ml) were added to each well. The fluorescence intensity (FI) of the lysis was analyzed using a microplate reader at λ_{ex}=458 and λ_{em}=505 nm. The same treatment was applied to the cells without the removal of the nanoparticles, which were used as the corresponding overall. Controls were prepared without the inhibitor pre-incubation at 37°C. The cell uptake efficiency was calculated according to Eq. 4.

Preparation of Caco-2 Cell Monolayers

Caco-2 cells were seeded onto polyester membrane filters (12 well, 0.45 μm, 1.12 cm^2) inside Transwell® chambers at a density of 1×10^5 cells/insert. The culture medium was replaced every other day. Cells were allowed to grow and differentiate in 21 days. The integrity of the monolayers was monitored by measuring the transepithelial electrical resistance (TEER) in HBSS using an Epithelial tissue voltohmmeter (EVOM^2, World Precision Instruments, Saratosa, FL, USA). Only cell monolayers with the TEER values above 500 Ω •cm^2 were used for the transport studies.

During the transport study, the integrity of cell monolayers was monitored by recording the TEER value. To evaluate TEER reversibility, the nanoparticles were incubated with Caco-2 cells for 2 h. After removing the nanoparticle samples, the monolayer was gently washed with HBSS and allowed to recover in DMEM-20 under culture conditions. Monolayer integrity was monitored by recording the TEER value for up to 24 h. The TEER was calculated according to Eq. (5): [20]

$$\text{TEER}\left(\Omega \cdot cm^2\right) = \left(R_{total} - R_{filter}\right) * A \tag{5}$$

where R_{total} and R_{filter} are the resistance values of the filter with cells (Ω) and without cells (Ω) respectively, and A is the surface of the Transwell® insert (cm^2).

Transport Efficiency of VB_{12}

Upon the equilibration at 37°C for 30 min, nanoparticle suspension or VB_{12} solution (0.5 ml) was added to the apical chamber and 1.5 ml HBSS was introduced to the basolateral chamber. The concentration of VB_{12} in each apical chamber was 1.5 μg/ml. After 22 h, the sample in basolateral chamber was collected into a centrifuge tube. The collected samples were concentrated at 25°C until dry using a Vacufuge® vacuum concentrator (Eppendorf AG, Barkhausenweg 1, Hamburg, Germany). A proper volume of 0.05% SDS (w/v) was added to each sample to dissociate nanoparticles and release

VB_{12}. [13, 14] The amount of VB_{12} was measured using the Reverse-phase high performance liquid chromatography (RP-HPLC). RP-HPLC was performed with a Kinetex^{TM} C_{18} column (4.6×150 mm, with a 1,200 Series Binary HPLC System (Agilent Technologies, Waldbronn, Germany) equipped with a G1312A bin pump, and a G1315D DAD detector. Flow rate was set at 1.0 ml/min, the injection volume was 50 μl and the detector was set at 360 nm. VB_{12} standards were prepared ranging from 0.5 to 50 μg/ml in MilliQ water. Linear gradient elution with aqueous acetonitrile was done according to previous method. [21] The transport efficiency is defined as the amount of VB_{12} transport across per unit of cell monolayer.

Transport Mechanism Across Caco-2 Cell Monolayer

To study the transport mechanism of nanoparticles, Caco-2 cell monolayers were pre-incubated with the inhibitors for 30 min at 37°C. Colchicine (COL, 5 μg/ml) was used to block the clathrin-mediated and/or caveolae-mediated transcytosis pathways. Chlorpromazine hydrochloride (CPZ, 5 μg/ml), flilipin III (FLI, 5 μg/ml) and 10 μg/ml cytochalasin D (CyD, 10 μg/ml) were used to inhibit the clathrin-mediated transcytosis, caveolae-mediated transcytosis and macropinocytosis pathways, respectively [19]. Afterwards, the cell monolayers were gently rinsed 3 times with the HBSS. Subsequently, nanoparticle suspensions containing 1.6 μg/ml VB_{12} (0.75 ml) and HBSS (1.5 ml) were applied to apical and basolateral compartments, respectively. Solutions in basolateral compartments were collected after 6 h and subjected to a similar treatment as indicated in the Section of *Transport Efficiency of VB_{12}*, prior to quantification of VB_{12} by RP-HPLC. A similar temperature block at 4°C was also performed.

Cross-section of Caco-2 Monolayers

Upon the equilibrate at 37°C for 30 min, SPI-NP-1 nanoparticle suspension (0.75 ml, containing 1.6 μg/ml VB_{12}, w/v) was added to the apical compartment. After 2 or 4 h incubation at 37°C, Caco-2 cell monolayers were washed 3 times gently and pre-fixed with 2.5% glutaraldehyde and 2% paraformaldehyde solution overnight at 4°C, followed by washing 4 times with PBS, for 10 min per change. The cells were post-fixed with 1% osmium tetroxide (OxO_4 in 0.12 M cacodylate buffer, pH 7.2) for 1-h, washed with PBS for 10 min per change. Samples were dehydrated in 50, 70 and 90% ethanol, for 15 min in each solution and 3 times in 100% ethanol. The cell monolayers were infiltrated twice, for 2 h each time, firstly by replacing the 100% ethanol with an ethanol:spur mixture (1:1, v/v) and then with a pure spur resin. The cell monolayers, together with a polyester membrane, were then carefully cut into small pieces and carefully placed in molds filled with spur resin. The molds were incubated at 70°C overnight to allow the polymerization of resin. The resin sample block was trimmed, thin-sectioned to a thickness of 70 nm using a microtome (Reichert-Jung Ultracut E Ultramicrotome) and collected on Formvar-coated copper grids. These grids were stained by 4% uranyl acetate for 30 min and lead citrate for 7 min in a CO_2 free chamber. The samples were then blotted with a filter paper and air-dried. Samples were observed under the TEM at 140 kV.

Ex Vivo Intestinal Transport

The *ex vivo* study of the intestinal transport of VB_{12}-nanoparticles was performed using a modified Ussing chamber model. [22] The animal care and experimental procedures were conducted in accordance with the Canadian Council on Animal Care and approved by the University of Alberta Animal Care and Use Committee (Livestock). Male 10-week old Sprague Dawley rats were purchased from Charles River Laboratories (Wilmington, MA) and fed a standard chow diet (Laboratory chow 5001). Animals were given free access to food and water. On the day of the experiment, animals were anesthetized with isoflurance-oxygen mix (3.5%) and sacrificed by exsanguination. The jejunum was removed distal to the ligament of the Treitz and immediately placed in an ice-cold Krebs buffer supplemented with sodium L-glutamate (4.9 mM), disodium fumarate (5.4 mM), sodium pyruvate (4.9 mM) and D-glucose (11.5 mM) and continuously bubbled with O_2/CO_2 (95/5%). Individual segments were cut from the jejunum and mounted in modified Ussing chambers (Harvard Apparatus Inc, Holliston, MA). Each mounted area available for permeation was 1.15 cm^2. Tissues were allowed to equilibrate in 6 ml oxygenated Krebs buffer at 37°C for 30 min for the following experiments.

Followed by the equilibration, 3 ml of Krebs buffer in mucosal chambers was replaced by 3 ml solutions of SPI-NP-1 nanoparticles containing 1.13 and 2.50 μg/ml VB_{12}. VB_{12} solution was used as a control. Following incubation for 2 h, the jejunum tissues were frozen in liquid N_2 for VB_{12} analysis. The tissues were then weighed and homogenized in PBS solution. The PBS-tissue homogenates suspensions were ultrasonificated for 4 h and samples were then centrifuged at 10,000 g for 30 min and the supernatant was collected. The remaining pellet was resuspended in 1.0 ml of PBS solution, ultrasonificated a further 4 h and centrifuged. The supernatant fractions were pooled together after washing the pellet twice and then dried by a Vacufuge® vacuum concentrator at 25°C. The residue of the supernatant pellet was suspended in 200 μl of PBS containing 0.05% SDS solution and subjected to ultrasonification for 10 min, then centrifuged at 10, 000 g for 20 min. The supernatant was filtered through a 0.45 μm PVDF syringe filter and the amount of VB_{12} was quantitated by RP-HPLC as indicated above.

Histological Observation of Nanoparticles

Followed by the above equilibration, COUM-6 labeled SPI-NP-1 nanoparticles and VB_{12} solution were added in the mucosal chamber. The concentration of VB_{12} in each sample was 1.6 μg/ml. After incubating for 2 h, tissues were carefully removed for histology observation. A small piece was cut from each segment and immediately mounted in OCT embedding media (Lamb-OCT, Thermo Scientific) on dry ice. Upon frozen, tissue blocks were stored at −20°C until cryosection. The sectioned tissues were mounted on glass slides using Prolong® Gold Anitfade reagent with DAPI staining and then observed with a CLSM as indicated in the Section *of CLSM Study*. The number of jejunum segments for SPI-NP-1 and VB_{12} was 3, obtained from 1 rat.

Statistical Analysis

All measurements were performed a minimum of 3 times. Data were represented as mean ± standard deviation (SD). Student's *t*-test was used for comparisons between two samples and one-way ANOVA for more than two samples.

RESULTS AND DISCUSSION

Preparation and Characterization of VB_{12}-loaded SPI Nanoparticles

VB_{12} was encapsulated upon the formation of SPI nanoparticles induced by calcium. [13] It has been demonstrated that VB_{12} can be confined in a three-dimensional network of soy protein mainly *via* hydrophobic interactions. [14] Particles with a similar surface charge of around −17 mV and different diameters of approximately 30, 100 and 180 nm, depending on the solution pH value and Ca^{2+} concentration, were obtained as determined by Zetasizer (Table I), these were coded as SPI-NP-1, SPI-NP-2 and SPI-NP-3, respectively. The loading capacity (LC) of the nanoparticles was around 10.28–13.47% with the loading efficiency (LE) of 0.021–0.030%. LC and LE were significantly elevated when particle size increased from 30 to 100 nm ($p<0.01$), however, the level of LC and LE did not change significantly ($p>0.05$) when particle size increased from 100 to 180 nm. The Recommended Dietary Allowances (RDAs) of VB_{12} for an adult is 2.4 μg per day [23]. In order to load 2.4 μg VB_{12}, 11.4, 12.3 and 14.3 mg SPI-NP-1, SPI-NP-2 and SPI-NP-3 particles will be needed based on the LC value in Table I, which is suitable for oral applications.

The TEM images of VB_{12}-loaded nanoparticles are shown in Fig. 1. The nanoparticles displayed a spherical shape, smooth surface and a relatively uniform size distribution. The mean size of nanoparticles was calculated based on their diameter in the TEM images,[24] and estimated to be smaller than the size analyzed by Zetasizer in Table I. The SPI-NP-2 nanoparticle, for example, had a size of 65 ± 9 nm in Fig. 1b; however, its size was around 99 ± 4 nm as measured by Zetasizer. The smaller size observed by TEM imaging may have been due to the shrinkage of nanoparticles during air drying prior to TEM observation [25].

Cytotoxicity of Nanoparticles

The toxicity of nanoparticles was evaluated using an XTT assay which assessed the activity of mitochondrial dehydrogenase as an indicator of viable cells. Fig. 2 shows that there was no significant effect of co-incubation of particle at each concentration on the viability of Caco-2 cells. The number of cells was also counted and consistent with the XTT assay ($p>0.05$, data not shown). This lack of toxicity to Caco-2 cells is likely attributed to the hydrophilic nature and good biocompatibility of SPI as previously reported [13].

In Vitro Cellular Uptake Profiles

Confluent Caco-2 cell monolayers form tight junctions and electrical properties that are similar to intact intestinal epithelium. [26] This cell line has been widely applied as a representative *in vitro* model for evaluating the uptake and transport properties of nanoparticles across the small intestinal epithelium for drug delivery [18, 27].

In order to investigate the association of nanoparticles with Caco-2 cells, SPI nanoparticles were labelled with green fluorescent probe (COUM-6) prior to CLSM observation. The labeling ratio of COUM-6 to SPI was 0.75 ± 0.06 ($\times 10^{-4}$):1 (w/w). The association of COUM-6 itself with cells was firstly examined under the CLSM (Fig. 3a), and no green fluorescent signal was detected indicating that this probe alone was not be internalized into Caco-2 cells in 6 h. [13, 18] However, strong green signal was observed at the periphery of cell nuclei following incubation with nanoparticles (Fig. 3b-d). Moreover, a brighter green signal was observed with the treatment of SPI-NP-2 nanoparticles, compared with those treated with SPI-NP-1 and SPI-NP-3 suggesting that particle size played an important role in the association of SPI nanoparticles with Caco-2 cells.

In order to further observe the location of nanoparticles in the cell, the cell was stained with WGA-Alex Fluor® 555 conjugate prior to CLSM observation in order to identify the cell membrane. Then three-dimensional analysis of the optical sections (z-axis) of the cell monolayer was performed to determine the intracellular distribution of nanoparticles. Figure 3e demonstrates that strong green signal was detected in the cytoplasm rather than around cell membrane. It suggests that majority of nanoparticles were accumulated in the

Table I Characteristics of VB_{12}-loaded SPI nanoparticles

Sample	Size (nm)	PDI	Zeta-potential (mV)	Loading capacity (%)	Loading efficiency (%)
SPI-NP-1	30 ± 1^a	0.27 ± 0.02	-17.9 ± 0.7^a	0.021 ± 0.002^a	10.28 ± 0.02^a
SPI-NP-2	99 ± 4^b	0.29 ± 0.03	-17.2 ± 0.2^a	0.026 ± 0.006^b	13.05 ± 0.06^b
SPI-NP-3	181 ± 3^c	0.31 ± 0.04	-16.3 ± 0.2^a	0.030 ± 0.002^b	13.47 ± 0.02^b

Data represent mean ± SD; ^{a,b,c} means significant difference at $p < 0.01$; PDI means polydispersity index.

cytoplasm (highlighted by white arrow heads). No nanoparticles were detected inside the cell nuclei as they may have been too large and this may have contributed to low toxicity as indicated by the XTT assay.

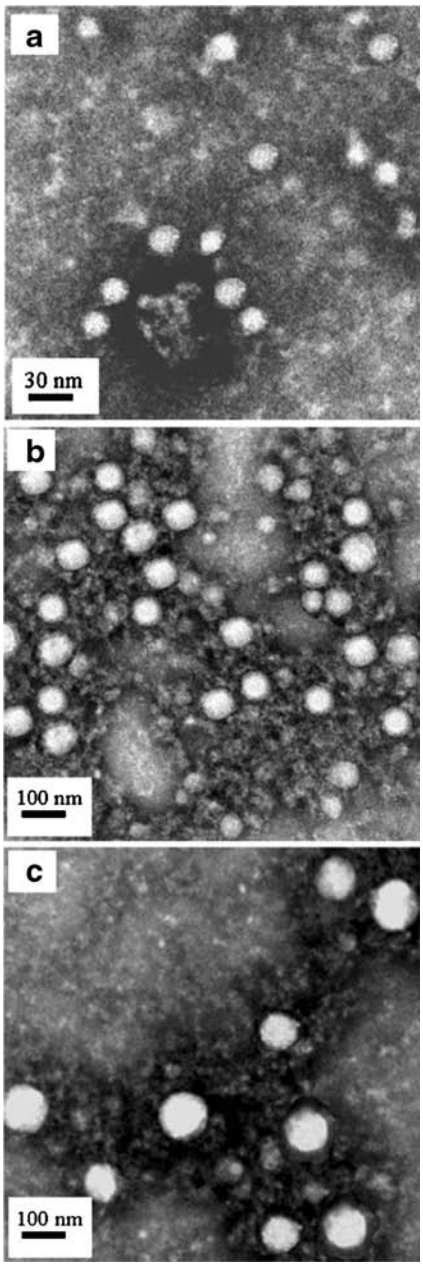

Fig. 1 TEM images of VB_{12}-loaded SPI nanoparticles of (**a**) SPI-NP-1; (**b**) SPI-NP-2; (**c**) SPI-NP-3.

As shown in Fig. 4a, the uptake efficiency of SPI nanoparticles by Caco-2 cells was in the order of 100 nm (SPI-NP-2) >30 nm (SPI-NP-1) >180 nm (SPI-NP-3) when their surface charge was fixed at −17 mV. Nanoparticles with a larger size need stronger driving forces and additional energy in the cellular internalization process. [27] This likely contributed to the cellular uptake of SPI nanoparticles significantly decreasing when size increased from 100 to 180 nm. The significant reduction in cellular uptake of particles from 100 to 30 nm ($p<0.01$) may be caused by different pathways of SPI nanoparticles being accumulated inside Caco-2 cells. It was reported that particles less than 50 nm could directly pass through paracellular spaces instead of being internalized through cell membranes. [28] Consequently, fewer particles were accumulated inside Caco-2 cells, resulting in the lower uptake efficiency of 30 nm particles.

The internalization of nanoparticles into Caco-2 cells was assessed by mean fluorescence intensity (MFI) of the three different sized nanoparticles inside Caco-2 cells is shown in Fig. 4b. A higher MFI means more nanoparticles internalization. In Fig. 4b, MFI significantly increased in the order of SPI-NP-2 > SPI-NP-1 > SPI-NP-3 ($p<0.05$) indicating that the internalization of nanoparticles was in the order of 100>

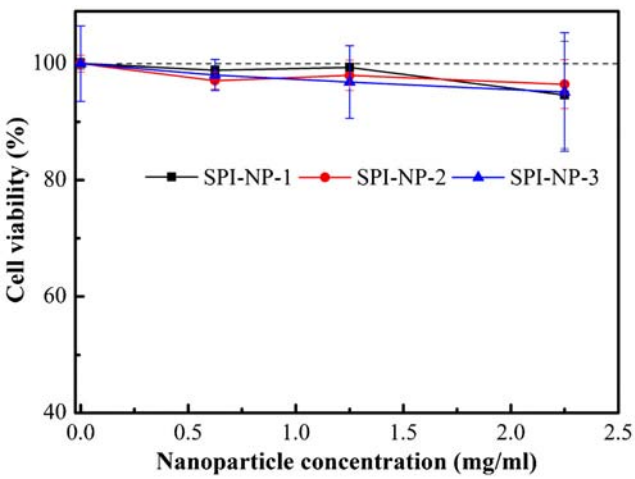

Fig. 2 The impacts of particles size on Caco-2 cell viability, analyzed by XTT assay. Nanoparticles were incubated with Caco-2 cells for 6 h at 37°C and the SPI nanoparticle concentration was in the range of 0.625–2.25 mg/ml. Data represented mean ± SD, $n=4$.

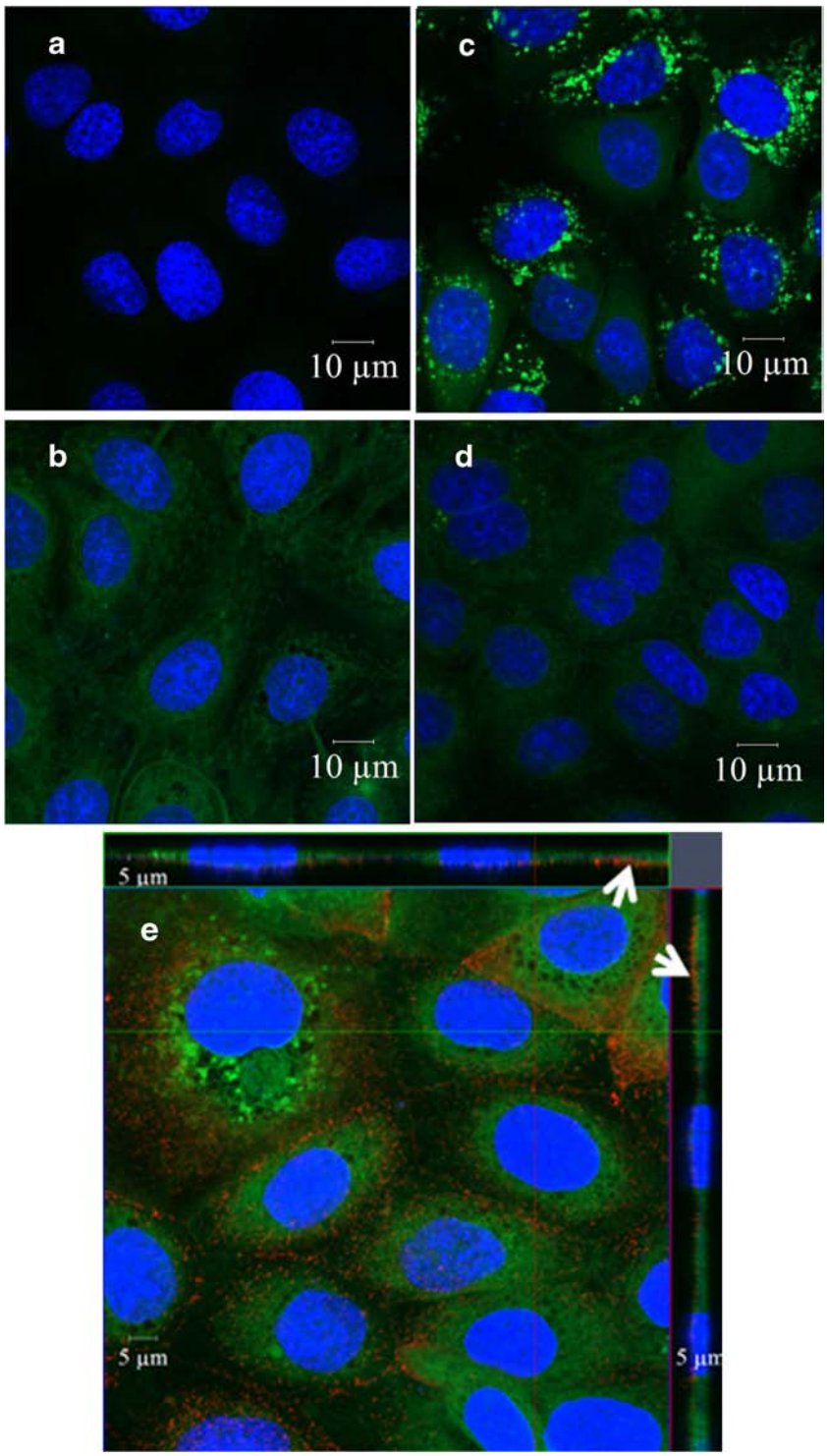

Fig. 3 CLSM images of Caco-2 cells after incubation with (**a**) COUM-6; (**b**) COUM-6 labeled SPI nanoparticles SPI-NP-1; (**c**) SPI-NP-2; (**d**) SPI-NP-3 at 37°C for 6 h; (**e**) localization of SPI nanoparticles within Caco-2 cells after incubation with SPI-NP-2 nanoparticles at SPI particle concentration of 1.25 μg/ml, 37°C for 4 h. White Arrow heads indicated the presence of the nanoparticles around cell membrane. Green: nanoparticles; blue: cell nuclei; red: cell membrane stained with WGA-Alex Fluor® 555 conjugate.

30>180 nm. This result was in good agreement with the cell uptake efficiency in Fig. 4a. Additionally, 100% of the Caco-2 cells showed the uptake of nanoparticles after 4 h as indicated by their FL I-H spectra were away from 10^1 (Fig. 4c).

A significant decrease in the uptake of nanoparticles by Caco-2 cells was observed at 4°C ($p<0.001$, Fig. 5a). This may be explained by lower metabolic activity of the cells and decreased fluidity of the cell membrane at this low temperature compared to 37°C, leading to a possible restriction in the passive permeability and/or energy-dependent transcellular processes. [27, 29] Despite a significant decrease in cellular uptake of nanoparticles at 4°C, 8.8–21.4% SPI nanoparticles were still taken up at this temperature (Fig. 5a). This may have

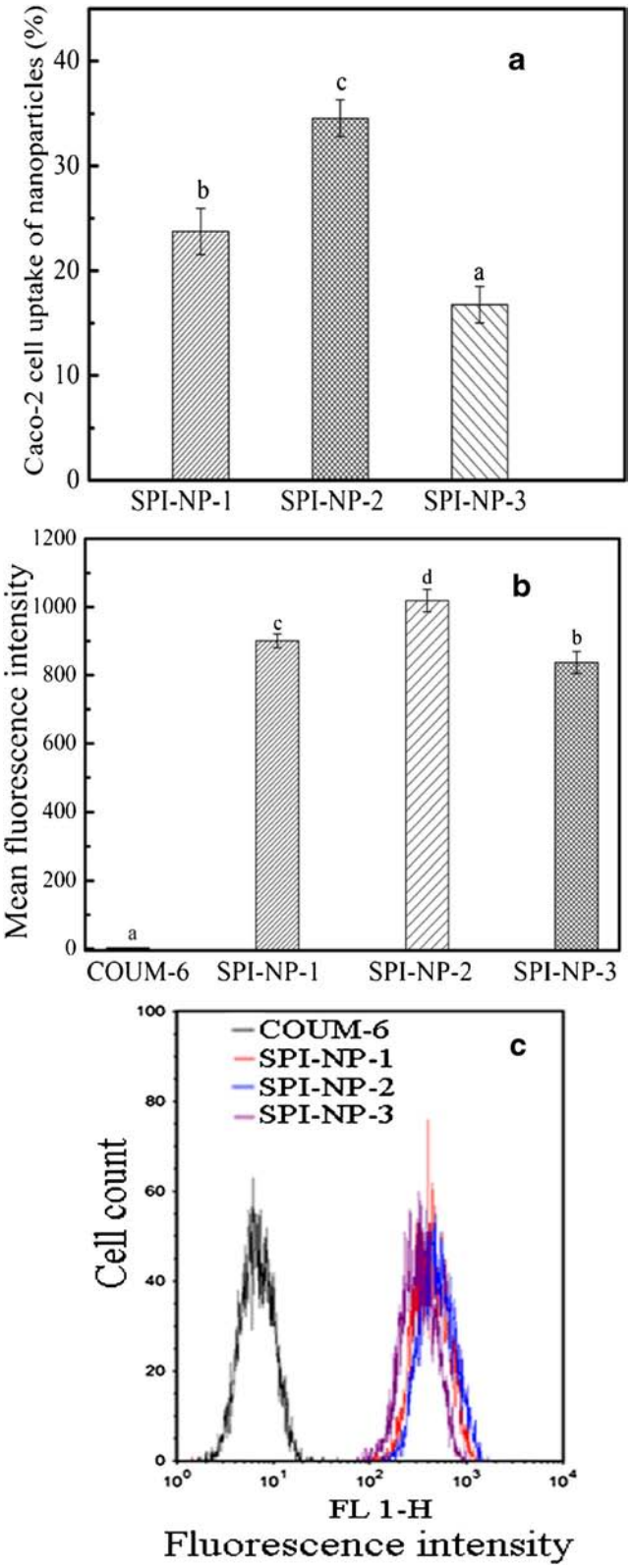

◀ **Fig. 4** (**a**) Effect of particle size on cellular uptake efficiency of SPI nanoparticles by Caco-2 cells. Data represented mean ± SD, $n = 4$; Significant difference was expressed as ^{a,b,c} at $p < 0.01$; (**b**) Flow cytometry analysis of cellular uptake of COUM-6 labeled SPI nanoparticles by Caco-2 cells. Data were presented as mean ± SD, $n = 3$. Significant difference was expressed as ^{a,b,c,d} at $p < 0.05$; (**c**) Flow cytometry analysis of mean fluorescence intensity of COUM-6 and COUM-6 labelled SPI nanoparticles in Caco-2 cells. Nanoparticles of a concentration of 1.25 mg/ml were incubated with cells for 4 h at 37°C.

been due to the physical adhesion and the passive diffusion of nanoparticles [30].

As shown in Fig. 5b, a combination of linear uptake (<4 h) and saturable uptake (>4 h) of SPI nanoparticles was observed suggesting that the cellular uptake of SPI nanoparticles may occur *via* macropinocytosis and receptor-mediated endocytosis pathways. [31, 32] The uptake of nanoparticles was again in the increasing order of SPI-NP-2 > SPI-NP-1 > SPI-NP-3 during the same time interval.

The combination of linear uptake at lower concentrations of SPI nanoparticles (0 to 2.0 mg/ml) and an apparent saturated uptake at higher concentrations (2.0 to 2.25 mg/ml) of SPI nanoparticles was observed. It supports the notion that cellular uptake of particles was through macropinocytosis and receptor-mediated endocytosis routes. [31, 32] At each concentration point, the order of cellular uptake of nanoparticles was SPI-NP-2 > SPI-NP-1 > SPI-NP-3.

NaN_3 is a metabolic inhibitor which blocks the production of ATP in cells and inhibits the endocytosis of nanoparticles. [33] The treatment of NaN_3 led to a significant decrease in the cellular uptake of SPI nanoparticles (Fig. 5d), confirming that the uptake of these nanoparticles was mainly through energy-dependent endocytosis. [27] However, there was not complete inhibition of uptake with the NaN_3 treatment, which suggests there is an energy-independent or passive component to the transport of nanoparticles into the cells [34].

Taken together, the cellular uptake behavior of SPI nanoparticles was saturable, temperature-, time-, concentration-dependent indicating that their uptake mechanisms by Caco-2 cells were predominantly by the energy-dependent endocytosis [35] and a smaller portion of uptake by passive transport.

Understanding the endocytosis processes of nanoparticles could allow researchers to bioengineer a highly specialized delivery system in order to achieve optimized uptake efficiency. Energy dependent uptake by enterocytes can be divided into: clathrin-mediated endocytosis, caveolae-mediated endocytosis, clathrin-/caveolae-independent endocytosis, and macropinocytosis. [19] Clathrin-mediated endocytosis leads to an intracellular pathway in which endosomes fuse with lysosomes to degrade their contents. Caveolae-mediated endocytosis avoids the lysosomal degradation and thus it is the most promising pathway for the transport of some vulnerable compounds into the enterocyte. [36] In macropinocytosis, the filling of the pocket occurs in a non-specific manner induced by electrostatic interactions, hydrophobic interactions, H-bonding, *etc.* [37].

COL is an inhibitor of caveolae-mediated and/or clathrin-mediated endocytosis. It inhibits actin polymerization and

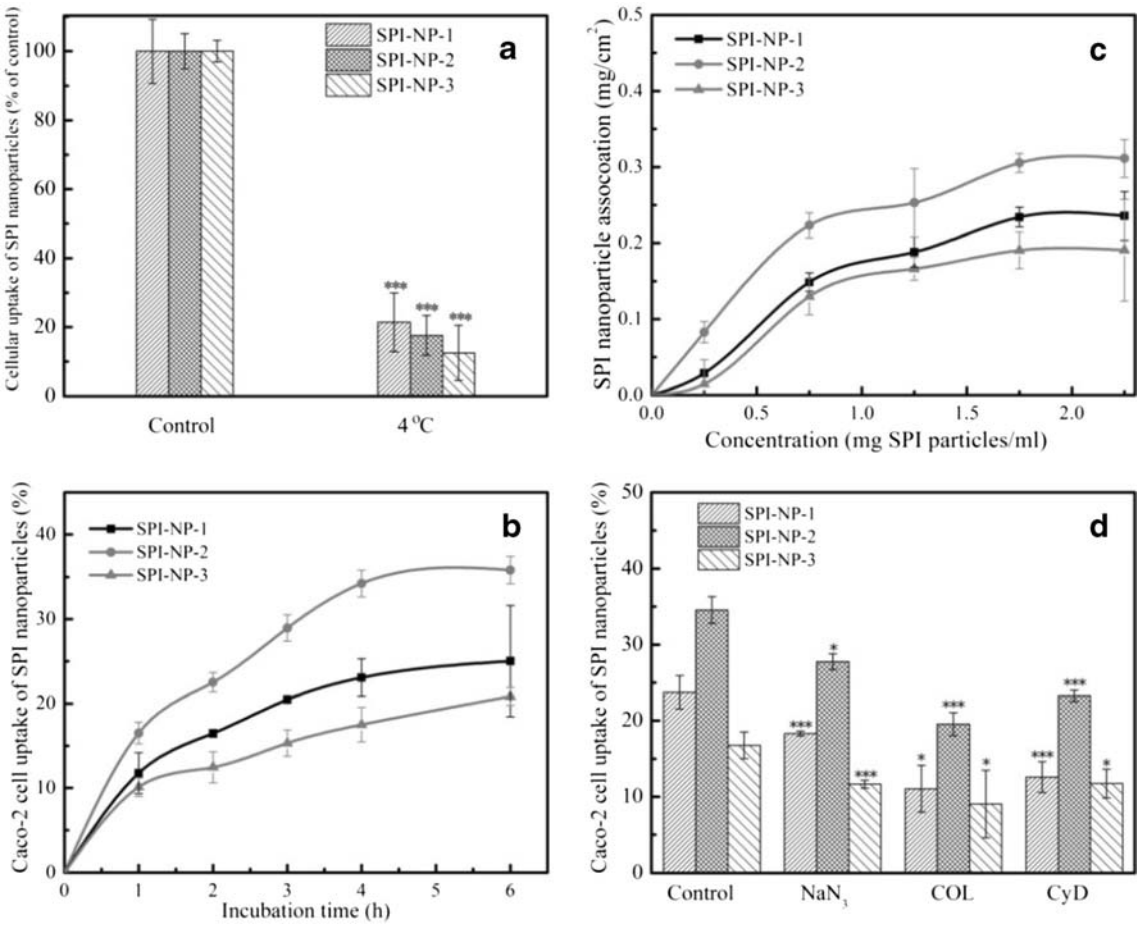

Fig. 5 The effects of (**a**) temperature block at 4°C, (**b**) incubation time, (**c**) particles concentration and (**d**) inhibitors on Caco-2 cell uptake efficiency of SPI nanoparticles with different sizes. Data represented mean ± SD, $n = 3$; *: $p < 0.05$; **: $p < 0.01$; ***: $p < 0.001$ (compared to the control of each type).

rearrangement for the formation and invagination of coated pits and caveosomes [38]. The presence of COL caused a remarkable decrease in cellular uptake of SPI nanoparticles as shown in Fig. 5d. It suggests a clathrin- and/or caveolae-mediated endocytosis was involved in the cellular uptake of SPI nanoparticles. CyD inhibits the macropinocytosis/phagocytosis by blocking the F-actin polymerization and membrane ruffling [39]. Since Caco-2 cell lines are considered to be non-phagocytic cells [40], the inhibition of VB_{12} transport by CyD would only reflect the role of macropinocytosis. The addition of CyD caused a significant decrease in the uptake of SPI nanoparticles suggesting cellular association with these nanoparticles was regulated by macropinocytosis as well. No remarkable differences were noticed in the uptake pathways of nanoparticles with a diameter of 30–180 nm.

The multiple endocytosis pathways of SPI nanoparticles together with their high cellular uptake efficiency indicate that SPI nanoparticles have the potential to improve the intestinal transport of VB_{12}. The apparent use of the multiple transport pathways may allow us to further optimize SPI nanoparticles with preferential targeting sites and improved bioavailability of the compound encapsulated.

RP-HPLC Method for VB_{12} Quantification

When cultured on permeable inserts, Caco-2 cells are able to spontaneously differentiate and polarize, forming a continuous monolayer in 21 days. The impact of particle size on the apical-to-basolateral transport of VB_{12} across the Caco-2 cell monolayers was evaluated, where free VB_{12} was used as a control. As shown in Fig. 6a, the transport of VB_{12} without encapsulation was 0.25 ± 0.015 μg/cm^2 following 22 h of incubation. After nanoencapsulation, VB_{12} transport increased to 0.80 ± 0.012, 0.61 ± 0.016, and 0.48 ± 0.033 μg/cm^2 for the particles of SPI-NP-1 (30 nm), SPI-NP-2 (100 nm) and SPI-NP-3 (180 nm), respectively. These findings indicate the transport efficiency of VB_{12} was significantly enhanced after being loaded into SPI nanoparticles *($p < 0.05$)*. This may be attributed to the combination of several physicochemical properties of particles such as size, surface hydrophobicity and charge, as well as matrix nature. [7] The surface carboxyl

groups have also been reported to facilitate the association of nanoparticles with cells. [38] Besides, certain peptides such as RGD (arginine-glycine-aspartate) derivatives on the particle surface may be able to activate the transport mechanisms in Caco-2 cells. [7, 41] SPI nanoparticles that are mild negatively charge (−17 mV) are more favorable for drug/nutraceuticals delivery, and positively charged particles tend to be toxic and immunogenic due to the strong interactions with negatively charged cell membranes or serum proteins [33].

From Fig. 6a, smaller sized nanoparticles (30 nm) demonstrated significantly greater VB_{12} transport efficiency, possibly due to the larger surface area to interact with the Caco-2 cell membranes. [42] Interestingly, in the uptake test (Fig. 4a), 30 nm particles exhibited a lower cellular uptake efficiency compared with 100 nm ones ($p < 0.05$). This may be explained by the fact that more particles were transported across Caco-2 basolateral barrier, thus fewer particles were left inside Caco-2 cells. This led to a higher transport efficiency across Caco-2 cell monolayer, but a lower uptake efficiency of 30 nm particles, compared with 100 nm ones. Their difference may be also caused by their transport pathways, which needs further investigation.

Transport Mechanism of Nanoparticles Across Caco-2 Cell Monolayers

Theoretically, nanoparticles can cross the epithelium by: 1) the paracellular pathway *via* tight junctions; 2) the transcellular pathway (passive or active) *via* the intestinal cells, being the most commonly studied and 3) lymphatic uptake (phagocytosis) *via* micro-fold (M) cells of Peyer's patches. [43, 44] Although intensive research on M-cells transport of nanoparticles has been done for drug delivery systems, M-cells represent less than 1% of the human intestinal epithelial cells and this pathway was not explored in this study.

The paracellular transport of particles is passive and results from diffusion and is limited by the tightness and tiny pore size of junctions between the epithelial cells. [44] Consequently, the tight junctions must be wide enough or opened up to facilitate the transport of nanoparticles. After exposure of

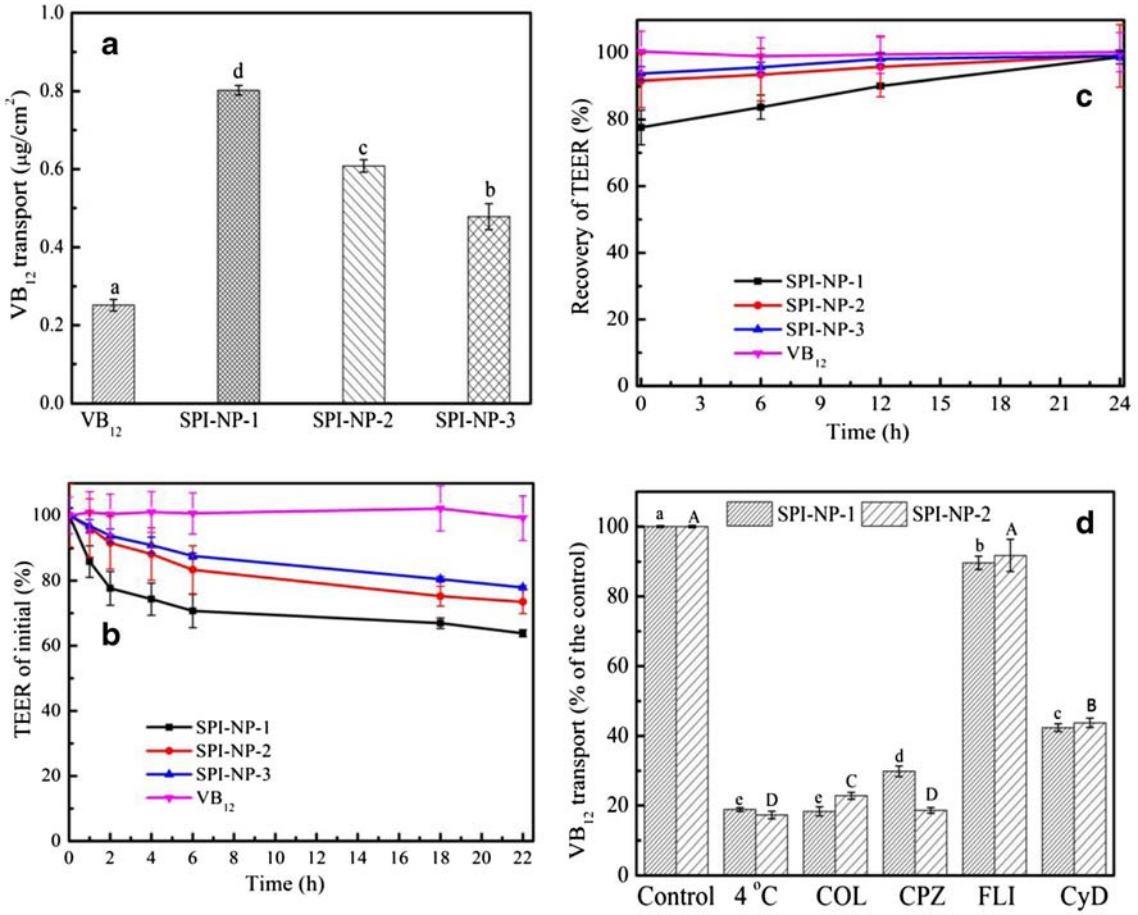

Fig. 6 (**a**) The impact of particle size on the accumulative transport of VB_{12} in SPI nanoparticle systems across the epithelial barrier from the apical chamber to the basolateral chamber at 37°C for 22 h. Data represent mean ± SD, $n = 3$. Significant difference was expressed as ^{a,b,c,d} at $p < 0.05$. (**b**) Effect of particle size on the transepithelial electrical resistance (TEER). (**c**) The recovery of TEER of Caco-2 cell monolayers as a function of time. (**d**) The impacts of temperature and inhibitors on the transport of VB_{12} across Caco-2 cell monolayers. Data represent mean ± SD, $n = 3$. Significant difference was expressed as ^{a,b,c,d} or ^{A,B,C,D} at $p < 0.05$.

nanoparticles to the Caco-2 cell monolayers, the TEER decreased by 22–36% at time 22 h, suggesting the opening of the tight junctions (Fig. 6b). The progressive decline in TEER with increased incubation time indicated the prolonged interactions of nanoparticles with the epithelial surface. The integrity and function of tight junctions depend on the extracellular Ca^{2+} and Mg^{2+},[45] which can be chelated by free carboxyl groups at the C-terminal of polypeptide chains or of acidic amino acids (Aspartate and Glutamate) in SPI nanoparticles. SPI nanoparticles were formed by using Ca^{2+} as a salt-bridge between two carboxyl groups, and less Ca^{2+} was introduced in smaller sized SPI-NP-1 (2.5 mM), compared with larger sized SPI-NP-2 (5 mM), to interact with carboxyl groups. [13] Accordingly, more free carboxyl groups was left on smaller particles, which could chelate more Ca^{2+}/Mg^{2+}, and thus leading to a greater decrease in the TEER value (Fig. 6c). The greater decrease in TEER on exposure to 30 nm particles, compared with 100 and 180 nm particles, was most likely due to the smaller size and permeability through the paracellular route [28].

The decreased in TEER on exposure to SPI nanoparticles could also suggest damage to the tight junctions which would cause increased nanoparticle permeability into the intestinal submucosa and possibly lead to an inflammatory or immunologic responses. [46] Although the inflammation was not measured in this study, the TEER recovered nearly completely in 24 h after removal of nanoparticles (Fig. 6c), suggesting SPI nanoparticles may transiently and reversibly increase the opening or damage the tight junctions to increase the permeability of particles in Caco-2 cell monolayers. The use of paracellular pathways are beneficial for the translocation of bioactive compounds, particularly as there are no proteolytic enzymes in the intercellular spaces. [47] The transport efficiency of nanoparticles, however, *via* the paracellular pathway is severely restricted by the limited surface area of tight junctions (<1% of the mucosal surface area) and the size of tight junction pores between the epithelial cells [48].

The cell membrane of enterocytes is an efficient targeting area for nanoparticle delivery, as it contributes to more than 90% of epithelial surface spaces. [44] In transcellular transport pathways, nanoparticles can pass through the cell membrane by passive diffusion or active transcytosis. The active transcytosis of nanoparticles can be blocked by dropping incubation temperature to 4°C. SPI-NP-1 and SPI-NP-2 were selected to investigate their transport mechanisms because they had greater VB_{12} transport efficiency, compared with SPI-NP-3. As shown in Fig. 6d, the transport efficiency of VB_{12} in all the nanoparticles significantly decreased at 4°C compared with the corresponding control at 37°C. This further suggests that active transcytosis was the predominant pathway for the transport of SPI nanoparticles. [19] However, even at 4°C, 20% of VB_{12} in all the particles passed through Caco-2 cell monolayers, suggesting paracellular transport and passive diffusion also occurred at this temperature [49].

The active transcytosis mechanisms could be subdivided into clathrin-mediated, caveolae-mediated, clathrin-/caveolae-independent, and macropinocytosis pathways. [19] As shown in Fig. 6d, treatment of Caco-2 cell monolayers with COL led to a significant reduction in VB_{12} transport in SPI-NP-1 and SPI-NP-2 systems ($p<0.05$), indicating that clathrin- and/or caveolae-mediated pathways were involved in the transcytosis of these nanoparticles. In order to determine the specific pathway, the inhibitors of CPZ and FLI with Caco-2 monolayers were also applied. CPZ blocks clathrin-mediated endocytosis *via* a mechanism, where adaptor complex 2 (AP2) and clathrin are redistributed away from the plasma membrane, making clathrin unavailable for assembly at the cell surface [50]. The treatment of CPZ induced a significant decrease in VB_{12} transport ($p<0.05$) in the samples of SPI-NP-1 and SPI-NP-2, suggesting that the clathrin-mediated pathway played a main role in the transcytosis of both 30 and 100 nm SPI nanoparticles. FLI interacts with 3-β-hydroxysterol in the plasma membrane to form filipin-sterol complexes. The complexes consequently disassemble the caveolae-1 coat, leading to a block of the caveolin-mediated pathway but without blocking the clathrin-mediated pathway [50]. The FLI treatment led to 10% reduction in the VB_{12} transport in SPI-NP-1 nanoparticles, compared with the control. However, no reduction was observed in the SPI-NP-2. This result suggests that the caveolae-mediated route played a role in the transcytosis of 30 nm nanoparticles. This pathway may contribute to a higher VB_{12} transport in SPI-NP-1, compared with that in SPI-NP-2 (Fig. 6a). In addition, the VB_{12} transport dropped off remarkably with the treatment of CyD ($p<0.05$), suggesting that macropinocytosis also played a main role in the transcytosis of SPI-NP-1 and SPI-NP-2 nanoparticles. In summary, the transcytosis of 30 and 100 nm SPI nanoparticles appears to be primarily regulated by clathrin-mediated transcytosis and macropinocytosis routes. Besides, caveolae-mediated transcytosis was involved in the transcytosis of 30 nm nanoparticles. In the Section of *In Vitro Cellular Uptake Profiles*, our findings indicate that clathrin- and/or caveolae-mediated transport and macropinocytosis were the main mechanisms involved in the endocytosis of 30 and 100 nm nanoparticles. It suggests that their endocytosis and transcytosis shared the clathrin-mediated and macropinocytosis pathways.

Intracellular trafficking of SPI-NP-1 nanoparticles was studied by monitoring SPI nanoparticles inside Caco-2 cells at different time intervals using TEM imaging. From the cross-section of Caco-2 cells, particles with a diameter of approximately 20–25 nm were observed at a high density inside cells at the time of 2 and 4 h (Red arrow, Fig. 7b-c), compared to time 0 h (Fig. 7a). Furthermore, a decreased density of nanoparticles was detected at 4 h compared with

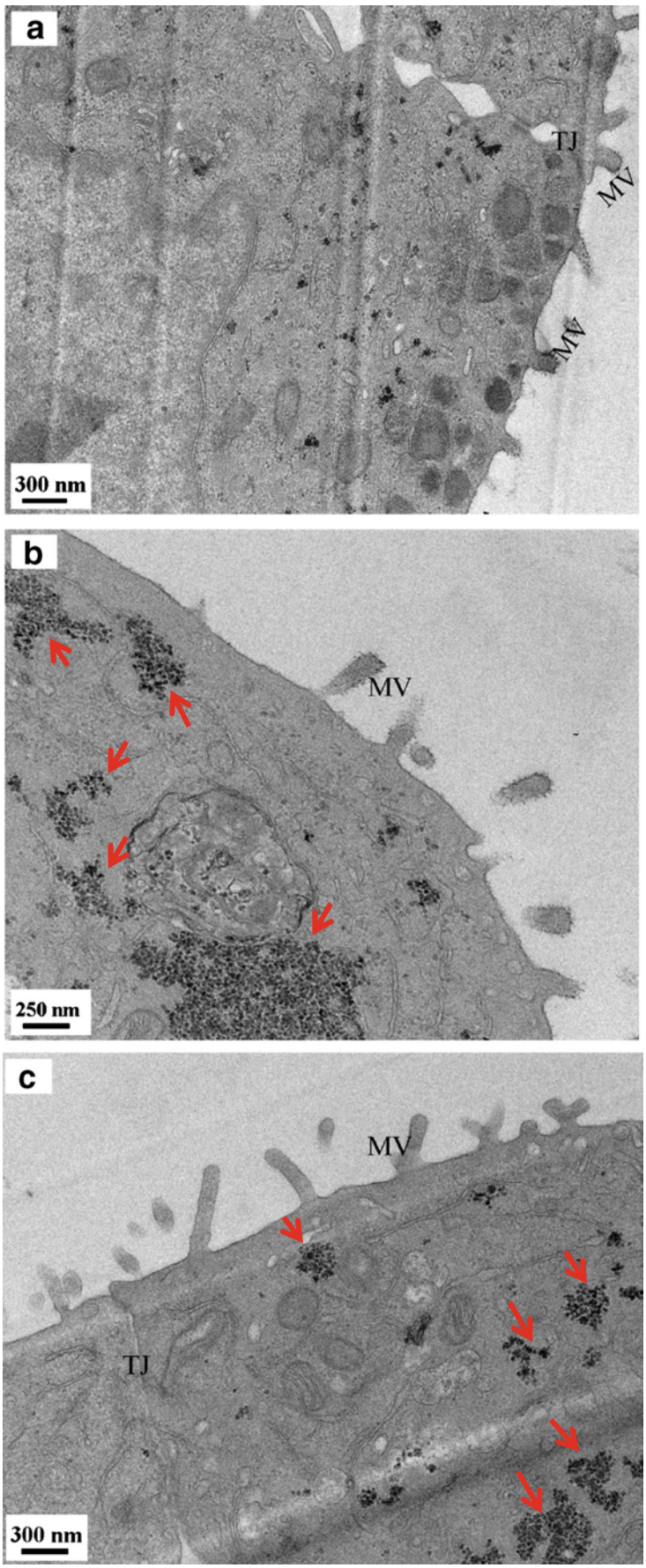

Fig. 7 TEM micrographs of Caco-2 cell monolayers on Transwell inserts incubated with SPI-NP-1 for (**a**) 0, (**b**) 2 and (**c**) 4 h at 37°C. Arrow heads show nanoparticles were accumulated within cells. TJ: tight junction; MV: microvilli.

that at 2 h suggesting nanoparticles were either degraded by lysosomes or transported through the basolateral membrane (exocytosis). Accordingly, it could be concluded that these high density particles were mostly from the exogenous SPI-NP-1 nanoparticles. This finding again indicates that nanoparticles could be internalized into Caco-2 cells. Furthermore, nanoparticles with a less density was observed at 4 h, compared with that at 2 h, suggesting nanoparticles were either degraded inside the lysosome or transported through the basolateral membrane (exocytosis).

The internalization of SPI-NP-1 and SPI-NP-2 nanoparticles by clathrin-mediated and macropinocytosis routes would typically end up in the endolysosomal pathway. Consequently, nanoparticles would be fused with lysosomes, where nanoparticles would likely be broken down by acid hydrolase enzymes. [37] In this case, VB_{12} could be released to the cytoplasm,

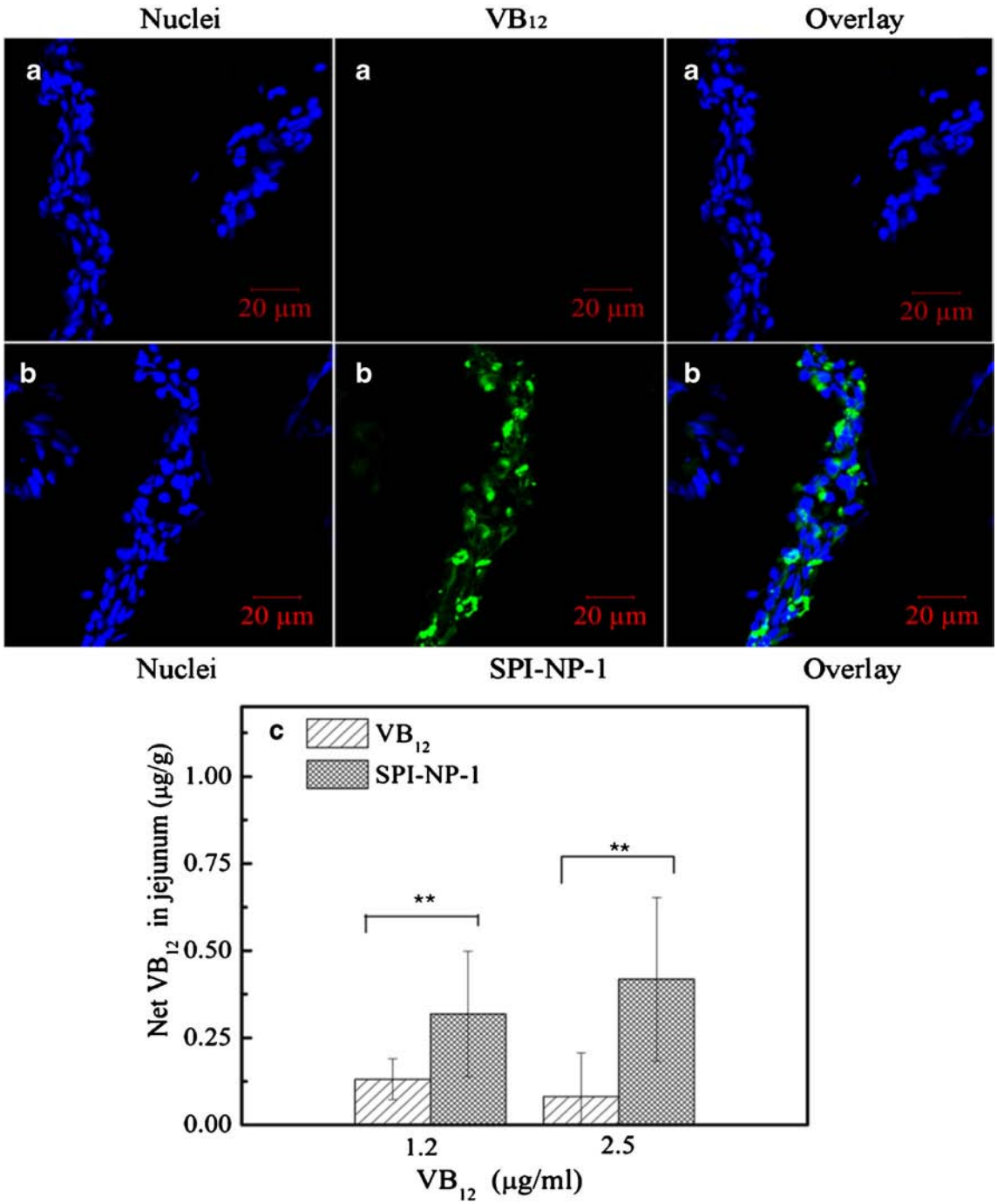

Fig. 8 Confocal images of rat jejunum incubated with (**a**) VB_{12} (a control) and (**b**) SPI-NP-1 nanoparticles for 2 h 37°C using Ussing chamber model. (**c**). The absorption of VB_{12} by rat jejunum in 2 h at 37°C. Data represented mean ± SD, $n = 15$ and $n = 9$ of SPI-NP-1 and VB_{12}, respectively; $^{**}p < 0.01$.

where it would be further reduced to active coenzymes, methylcobalamin or *S*-adenosylcobalamin and be available for cellular functions. [51] In contrast, the internalization of SPI-NP-1 *via* caveolae-mediated transcytosis pathway could avoid particles and VB_{12} endolysosomal degradation. Moreover, the transport of SPI nanoparticles *via* paracellular pathway could also avoid intracellular degradation of VB_{12}. Both pathways may be responsible for higher VB_{12} transport in SPI-NP-1, compared with SPI-NP-2 and SPI-NP-3.

Ex Vivo Intestinal Transport

The transport of nanoparticles was studied in rat jejunum model using an *ex vivo* Ussing chamber technique. SPI-NP-1 nanoparticle was selected because of the optimized VB_{12} transport efficiency across Caco-2 cell monolayers (Fig. 6a). As shown in CLSM images in Fig. 8a-b, the green SPI-NP-1 nanoparticles were shown to be permeable into the jejunal enterocyte and were distinguishable from the blue nuclei after 2 h incubation with mucosal side of the jejunum, indicating that SPI nanoparticles could be absorbed by intestinal tissue.

The amount of VB_{12} in the jejunum tissue was measured by RP-HPLC after incubation with SPI-NP-1 nanoparticles for 2 h at 37°C, with VB_{12} solution used as a control. As shown in Fig. 8c, SPI-NP-1 nanoparticle delivery of VB_{12} was 3–4 fold higher compared to the VB_{12} solution ($p<0.01$), 0.42 ± 0.24 and 0.08 ± 0.13 μg VB_{12} per g of jejunum, respectively for the 2.5 μg/ml dose of VB_{12}. These data suggest that SPI nanoparticles enhanced the intestinal transport and uptake of VB_{12}, consistent with the cell culture studies.

To sum up, the absorption of VB_{12} is a complex process, which only occurs in the distal ileum [1]. SPI nanoparticles could potentially carry VB_{12} across the intestinal barriers mainly *via* clathrin-mediated and macropinocytosis pathways compared to its original complex pathway, leading to increased VB_{12} absorption in the whole small intestine.

CONCLUSIONS

Mild negatively charged VB_{12}-loaded SPI nanoparticles with different sizes were successfully prepared without using any organic solvent. SPI nanoparticles containing VB_{12} significantly improved VB_{12} transport in *in vitro* and *ex-vivo* tissue studies. SPI nanoparticles appeared to be taken up *via* clathrin-mediated endocytosis and macropinocytosis pathways which may improve intestinal transport of VB_{12} in conditions of potential VB_{12} deficiency. Further dietary *in vivo* studies are required to test the efficacy of SPI nanoparticle intestinal delivery of VB_{12} to improve VB_{12} bioavailability.

ACKNOWLEDGMENTS AND DISCLOSURES

We are grateful to the Natural Sciences and Engineering Research Council of Canada (NSERC) for financial support and Canada Foundation for Innovation (CFI) for equipment support. Jing Zhang thanks the China Scholarship Council for providing a scholarship for her PhD program. The authors thank Mr. Jingzhou Huang for helping with Flow cytometry. The authors also thank Dr. Xuejun Sun and Ms. Geralidine Barron for their assistance with Confocal laser scan microscopy and Ms. Arlene Oatway for help with TEM.

REFERENCES

1. Kozyraki R, Cases O. Vitamin B_{12} Absorption: mammalian physiology and acquired and inherited disorders. Biochimie. 2013;95:1002–7.
2. Allen RH, Seetharam B, Podell E, Alpers DH. Effect of proteolytic enzymes on the binding of cobalamin to r protein and intrinsic factor: *in vitro* evidence that a failure to partially degrade protein is responsible for cobalamin malabsorption in pancreatic insufficiency. J Clin Investig. 1978;61(1):47.
3. Doets EL, Szczecińska A, Dhonukshe-Rutten R, Cavelaars A, van't Veer P, Brzozowska A, *et al.* Systematic review on daily vitamin B_{12} losses and bioavailability for deriving recommendations on vitamin B_{12} intake with the factorial approach. Ann Nutr Metab. 2013;62(4):311–22.
4. Sarti F, Iqbal J, Müller C, Shahnaz G, Rahmat D, Bernkop-Schnürch A. Poly (acrylic acid)-cysteine for oral vitamin B_{12} delivery. Anal Biochem. 2011;420(1):13–9.
5. Lin YH, Mi FL, Chen CT, Chang WC, Peng SF, Liang HF, *et al.* Preparation and characterization of nanoparticles shelled with chitosan for oral insulin delivery. Biomacromolecules. 2007;8(1):146–52.
6. Lin YH, Chen CT, Liang HF, Kulkarni AR, Lee PW, Chen CH, *et al.* Novel nanoparticles for oral insulin delivery *via* the paracellular pathway. Nanotechnology. 2007;18(10):105102.
7. des Rieux A, Fievez V, Garinot M, Schneider YJ, Préat V. Nanoparticles as potential oral delivery systems of proteins and vaccines: a mechanistic approach. J Control Release. 2006;116(1):1–27.
8. Livney YD. Milk proteins as vehicles for bioactives. Curr Opin Colloid Interface Sci. 2010;15(1):73–83.
9. Elzoghby AO, Samy WM, Elgindy NA. Protein-based nanocarriers as promising drug and gene delivery systems. J Control Release. 2012;161(1):38–49.
10. Teng Z, Luo YC, Wang Q. Nanoparticles synthesized from soy protein: preparation, characterization, and application for nutraceutical encapsulation. J Agric Food Chem. 2012;60(10):2712–20.
11. Teng Z, Luo Y, Wang Q. Carboxymethyl chitosan-soy protein complex nanoparticles for the encapsulation and controlled release of VitaminD_3. Food Chem. 2013;141(1):524–32.
12. Teng Z, Luo Y, Wang T, Zhang B, Wang Q. Development and application of nanoparticles synthesized with folic acid conjugated soy protein. J Agric Food Chem. 2013;61(10):2556–64.
13. Zhang J, Liang L, Tian Z, Chen L, Subirade M. Preparation and *in vitro* evaluation of calcium-induced soy protein isolate nanoparticles and their formation mechanism study. Food Chem. 2012;133(2):390–9.
14. Zhang J, Tian ZG, Liang L, Subirade M, Chen L. Binding interactions of β-conglycinin and glycinin with vitamin B_{12}. J Phys Chem B. 2013;117(45):14018–28.

15. Lee KD, Nir S, Papahadjopoulos D. Quantitative analysis of liposome-cell interactions *in vitro*: rate constants of binding and endocytosis with suspension and adherent J774 cells and human monocytes. Biochemistry. 1993;32(3):889–99.
16. Borges O, Cordeiro-da-Silva A, Romeijn SG, Amidi M, de Sousa A, Borchard G, *et al.* Uptake studies in rat Peyer's patches, cytotoxicity and release studies of alginate coated chitosan nanoparticles for mucosal vaccination. J Control Release. 2006;114(3):348–58.
17. Han J, Wang Q, Zhang Z, Gong T, Sun X. Cationic bovine serum albumin based self-assembled nanoparticles as siRNA delivery vector for treating lung metastatic cancer. Small. 2013;10(3):524–35.
18. Yin Win K, Feng S-S. Effects of particle size and surface coating on cellular uptake of polymeric nanoparticles for oral delivery of anticancer drugs. Biomaterials. 2005;26(15):2713–22.
19. Beloqui A, Solinís MÁ, Gascón AR, del Pozo-Rodríguez A, des Rieux A, Préat V. Mechanism of transport of saquinavir-loaded nanostructured lipid carriers across the intestinal barrier. J Control Release. 2013;166(2):115–23.
20. Déat-Lainé E, Hoffart V, Garrait G, Beyssac E. Whey protein and alginate hydrogel microparticles for insulin intestinal absorption: evaluation of permeability enhancement properties on Caco-2 cells. Int J Pharm. 2012;453(2):336–42.
21. Hugenschmidt S, Schwenninger SM, Lacroix C. Concurrent high production of natural folate and vitamin B_{12} using a co-culture process with lactobacillus plantarum SM39 and propionibacterium freudenreichii DF13. Process Biochem. 2011;46(5):1063–70.
22. Vine D, Charman S, Gibson P, Sinclair A, Porter C. Effect of dietary fatty acids on the intestinal permeability of marker drug compounds in excised rat jejunum. J Pharm Pharmacol. 2002;54(6):809–19.
23. Institute of Medicine. Food and Nutrition Board. Dietary reference intakes: thiamin, riboflavin, niacin, vitamin B6, folate, vitamin B12, pantothenic acid, biotin, and choline. Washington, DC: National Academy Press; 1998.
24. Akbari B, Tavandashti MP, Zandrahimi M. Particle size characterization of nanoparticles-a practical approach. Iran J Mater Sci Eng. 2011;8(2):48–56.
25. Pan X, Yu S, Yao P, Shao Z. Self-assembly of β-casein and lysozyme. J Colloid Interface Sci. 2007;316(2):405–12.
26. Hidalgo IJ, Raub TJ, Borchardt RT. Characterization of the human colon carcinoma cell line (Caco-2) as a model system for intestinal epithelial permeability. Gastroenterology. 1989;96(3):736–49.
27. He C, Hu Y, Yin L, Tang C, Yin C. Effects of particle size and surface charge on cellular uptake and biodistribution of polymeric nanoparticles. Biomaterials. 2010;31(13):3657–66.
28. Yin Win K, Feng SS. Effects of particle size and surface coating on cellular uptake of polymeric nanoparticles for oral delivery of anticancer drugs. Biomaterials. 2005;26(15):2713–22.
29. Liu Y, Wang P, Sun C, Feng N, Zhou W, Yang Y, *et al.* Wheat germ agglutinin-grafted lipid nanoparticles: preparation and *in vitro* evaluation of the association with Caco-2 monolayers. Int J Pharm. 2010;397(1):155–63.
30. Jiang L, Li X, Liu L, Zhang Q. Cellular uptake mechanism and intracellular fate of hydrophobically modified pullulan nanoparticles. Int J Nanomedicine. 2013;8:1825.
31. Catizone A, Medolago Albani L, Reola F, Alescio T. A quantitative assessment of non-specific pinocytosis by human endothelial cells surviving *in vitro*. Cell Mol Biol. 1993;39(2):155–69.
32. Panyam J, Dali MM, Sahoo SK, Ma W, Chakravarthi SS, Amidon GL, *et al.* Polymer degradation and *in vitro* release of a model protein from poly (d, l-lactide-co-glycolide) nano-and microparticles. J Control Release. 2003;92(1):173–87.
33. Bajaj A, Samanta B, Yan H, Jerry J, Rotello VM. Stability, toxicity and differential cellular uptake of protein passivated-Fe_3O_4 nanoparticles. J Mater Chem. 2009;19(35):6328–31.
34. Behrens I, Pena AIV, Alonso MJ, Kissel T. Comparative uptake studies of bioadhesive and non-bioadhesive nanoparticles in human intestinal cell lines and rats: the effect of mucus on particle adsorption and transport. Pharm Res. 2002;19(8):1185–93.
35. Lu W, Zhang Y, Tan YZ, Hu KL, Jiang XG, Fu SK. Cationic albumin-conjugated pegylated nanoparticles as novel drug carrier for brain delivery. J Control Release. 2005;107(3):428–48.
36. del Pozo-Rodriguez A, Pujals S, Delgado D, Solinís M, Gascón A, Giralt E, *et al.* A proline-rich peptide improves cell transfection of solid lipid nanoparticle-based non-viral vectors. J Control Release. 2009;133(1):52–9.
37. Bareford LM, Swaan PW. Endocytic mechanisms for targeted drug delivery. Adv Drug Deliv Rev. 2007;59(8):748–58.
38. He CB, Hu YP, Yin LC, Tang C, Yin CH. Effects of particle size and surface charge on cellular uptake and biodistribution of polymeric nanoparticles. Biomaterials. 2010;31(13):3657–66.
39. Harley VS, Dance DA, Drasar BS, Tovey G. Effects of burkholderia pseudomallei and other burkholderia species on eukaryotic cells in tissue culture. Microbios. 1997;96(384):71–93.
40. Luo Y, Teng Z, Wang TT, Wang Q. Cellular uptake and transport of zein nanoparticles: effects of sodium caseinate. J Agric Food Chem. 2013;61(31):7621–9.
41. Lin IC, Liang MT, Liu TY, Ziora ZM, Monteiro MJ, Toth I. Interaction of densely polymer-coated gold nanoparticles with epithelial Caco-2 monolayers. Biomacromolecules. 2011;12(4):1339–48.
42. Rieux A, Ragnarsson EG, Gullberg E, Préat V, Schneider YJ, Artursson P. Transport of nanoparticles across an *in vitro* model of the human intestinal follicle associated epithelium. Eur J Pharm Sci. 2005;25(4):455–65.
43. Rieux A, Ragnarsson EG, Gullberg E, Préat V, Schneider YJ, Artursson P. Transport of nanoparticles across an *in vitro* model of the human intestinal follicle associated epithelium. Eur J Pharm Sci. 2005;25(4):455–65.
44. Jung T, Kamm W, Breitenbach A, Kaiserling E, Xiao J, Kissel T. Biodegradable nanoparticles for oral delivery of peptides: is there a role for polymers to affect mucosal uptake? Eur J Pharm Biopharm. 2000;50(1):147–60.
45. Delie F, Rubas W. A human colonic cell line sharing similarities with enterocytes as a model to examine oral absorption: advantages and limitations of the Caco-2 model. Crit Rev Ther Drug Carrier Syst 1997;14(3)
46. Deitch E. Nutrition and the gut mucosal barrier. Curr Opin Gen Surg. 1992:85–91
47. Gaumet M, Gurny R, Delie F. Localization and quantification of biodegradable particles in an intestinal cell model: the influence of particle size. Eur J Pharm Sci. 2009;36(4):465–73.
48. Pappenheimer JR. Physiological regulation of transepithelial impedance in the intestinal mucosa of rats and hamsters. J Membr Biol. 1987;100(1):137–48.
49. Verma A, Uzun O, Hu Y, Hu Y, Han HS, Watson N, *et al.* Surface-structure-regulated cell-membrane penetration by monolayer-protected nanoparticles. Nat Mater. 2008;7(7):588–95.
50. Jiang M, Gan L, Zhu C, Dong Y, Liu J, Gan Y. Cationic core-shell liponanoparticles for ocular gene delivery. Biomaterials. 2012;33(30):7621–30.
51. Petchkrua W, Burns SP, Stiens SA, James JJ, Little JW. Prevalence of vitamin B_{12} deficiency in spinal cord injury. Arch Phys Med Rehabil. 2003;84(11):1675–9.